SoC-Based Droop Coefficients Stability Region Analysis of the Battery for Stand-Alone Supply Systems With Constant Power Loads

Rui Wang, *Student Member, IEEE*, Qiuye Sun, *Senior Member, IEEE*, Wei Hu, *Student Member, IEEE*,
Yushuai Li, *Member, IEEE*, Dazhong Ma, *Member, IEEE*, and Peng Wang, *Fellow, IEEE*

***Abstract*—The droop control is an advantageous approach for stand-alone supply systems consisting of multiple batteries, allowing among various inverters without intercommunication. The droop coefficients of batteries always vary with their state-of-charge (SoC) and charge/discharge mode, resulting in small-signal instability. Nevertheless, the existing impedance-based approaches can only assess the droop coefficients stability point, but not the stability region. Therefore, this article proposes a droop coefficients stability region analysis approach. First, the charge/discharge SoC-based droop controlled battery, the P&Q controlled distributed generator and the constant power load are separately discussed. Meanwhile, the state matrix and return-ratio matrix are established, respectively. Furthermore, the novel forbidden region criterion based on the return-ratio matrix is constructed, which reduces conservatism compared with norm-based impedance criteria and partial forbidden region criteria. Such a forbidden region criterion is first switched to the Hurwitz identification problem regarding the equivalent return-ratio matrix. Combined the state matrix and the equivalent return-ratio matrix, the generalized incidence matrix is constructed to simultaneously identify subsystem stability and interactive stability. Based on the generalized incidence matrix, an adaptive step search strategy is proposed to obtain the droop coefficients coordinated stability region. Finally, the simulation and experimental results illustrate the validity of the proposed method.**

***Index Terms*—Battery, droop control, generalized return-ratio matrix, stability region.**

I. INTRODUCTION

FOR remote location with difficult connect to the main grid, such as mountainous regions and remote villages, the stand-alone supply system has become an effective choice [1], [2]. Therein, distributed generators (DGs) have been widely applied to reduce fuel consumption and CO_2 emission. Meanwhile, energy storage systems such as batteries have been broadly utilized to compensate the power imbalance between the DGs and loads. Nevertheless, the low-frequency oscillation and harmonic oscillation accidents have been broadly reported in this stand-alone supply system. Especially when the loads are interfaced through the tightly regulated power electronics converters, and operate as constant power loads (CPLs) with a negative impedance characteristic, which causes the stand-alone supply system to be more prone to small-signal instability [3], [4].

Several global control strategies were implemented in the stand-alone supply system to achieve the energy management. On one hand, the central control or master–slave approach was proposed, which required a fast communication system between master and system elements [5]. On the other hand, the distributed control approach was proposed, where the battery inverters operated as voltage source inverters (VSIs) based on droop controllers and renewable energy source inverters operated as current source inverters (CSIs) based on P&Q controllers [5]–[7]. Based on this, the demand of communication module among VSIs was avoided, and CSIs performed maximum power point tracking during normal operation and reduced their power relying on the grid frequency. In order to balance state-of-charge (SoC) of distributed batteries in microgrids, the adaptive droop control was proposed, which caused the variation of droop coefficients [7]. Meanwhile, it was possible that the stand-alone supply system dominated by power electronics converters occurred small-signal instability phenomenon [8].

Two main approaches were presented to analyze the small-signal stability of the system dominated by power electronics converters, i.e., state-steady approach and impedance approach [9]–[20]. From the viewpoint of the state-steady approach, the small-signal state-steady function of the converters without voltage/current cascaded controller was built to assess the system stability in [9]. Furthermore, the full order state-steady function of the small-scale microgrid was established in [10]. The literature [11] built state-steady function of the ac–dc hybrid

Manuscript received January 28, 2020; revised August 22, 2020 and November 4, 2020; accepted January 1, 2021. Date of publication January 5, 2021; date of current version March 5, 2021. This work was supported in part by the National Key Research and Development Program of China under Grant 2018YFA0702200 and in part by the National Natural Science Foundation of China under Grants U20A20190 and 62 073 065. Recommended for publication by Associate Editor J. M. Guerrero. *(Corresponding author: Qiuye Sun.)*

Rui Wang is with the Northeastern University, Shenyang 110819, China, and also with the Energy Research Institute, Nanyang Technological University, Singapore 639798, Singapore (e-mail: 1610232@stu.neu.edu.cn).

Qiuye Sun, Yushuai Li, and Dazhong Ma are with the Northeastern University, Shenyang 110819, China (e-mail: sunqiuye@ise.neu.edu.cn; lysise@126.com; madazhong@ise.neu.edu.cn).

Wei Hu is with the College of Mechanical and Vehicle Engineering, Hunan University, Hunan 410082, China (e-mail: hithuwei@163.com).

Peng Wang is with the School of Electrical and Electronic Engineering, Nanyang Technological University Singapore 639798, Singapore (e-mail: epwang@ntu.edu.sg).

Color versions of one or more figures in this article are available at https://doi.org/10.1109/TPEL.2021.3049241.

Digital Object Identifier 10.1109/TPEL.2021.3049241

microgrid to solve the stability assessment problem regarding bidirectional power flow. There was no doubt that the stability analysis of the converter-dominated system was time-consuming [12], [13]. In order to reduce the computational burden, several model reduction approaches such as participation analysis [12], aggregate model [13], and so on, were proposed one after another. Obviously, it was still difficult to establish the state-space function of the complex power system [14]. As a result, the impedance approach was proposed to deal with the stability issue of the complex power system consisting of numerous converters. The impedance approach was based on the return-ratio matrix between the output source subsystem and the input load subsystem [15], [16]. Therein, the Nyquist criterion (NC) and generalized Nyquist criterion (GNC) were separately applied for the dc system and ac system to analyze system stability [16]. The literature [17] first proposed a sum type criterion to assess the stability of the power electronics converter with the bidirectional power flow. In order to deal with the mirror frequency coupled feature, the apparent impedance analysis approach and harmonic stability analysis approach were separately proposed [18], [19]. Nevertheless, the GNC was complex, and it was not suitable for the design of the ac system [20]. To solve this problem, several forbidden region criteria were proposed to eliminate the tedious drawing process of the generalized Nyquist curve in turn [21]. Likewise, the norm-based impedance criteria were also constructed to solve the limitation of the GNC [20]. Nevertheless, some problems have not be solved, which are shown as follows. First, there was no doubt that the artificial conservatism would be introduced in these two series criteria. Second, the impedance approach focused more on the interactive stability, rather than on the subsystem stability and dynamic characteristics of the single inverter itself [22]. Third, the classical impedance approaches paid more attention to the identification of stability operation points and the stability margin assessment of return-ratio matrix, and it could not provide detailed droop coefficients stability region.

To solve the foresaid three problems, this article proposes a droop coefficients stability region identification approach based on the generalized incidence matrix. The detailed features and advantages of this article are depicted as follows.

1) The modified stability forbidden region criterion is proposed in this article, which is further switched to the stability operation region criterion through mirror mapping. The proposed criterion has lower conservatism than the norm-based impedance criteria [20] and partial stability forbidden region criteria [21]. Meanwhile, the proposed criterion has similar conservatism with novel forbidden-region-based stability criterion (N-FRB criterion) [23].
2) The stability subregion is first switched as Hurwitz matrix space through the rotation mapping and translation mapping. With this effort, the interactive stability identification problem is transformed into the condition that at least one of these three equivalent return-ratio matrices is Hurwitz.
3) The generalized incidence matrix is first constituted to assess the subsystem stability and interactive stability at the same time through combining state matrix and equivalent return-ratio matrix, which results in that the solution process of the total stability region is switched as the stability boundary identification problem of the parameter-dependant nonlinear time-invariant matrix.
4) Based on the generalized incidence matrix, an adaptive step search strategy is proposed to obtain the droop coefficients stability region, providing the guidance for the energy management of batteries and stabilization method research works.

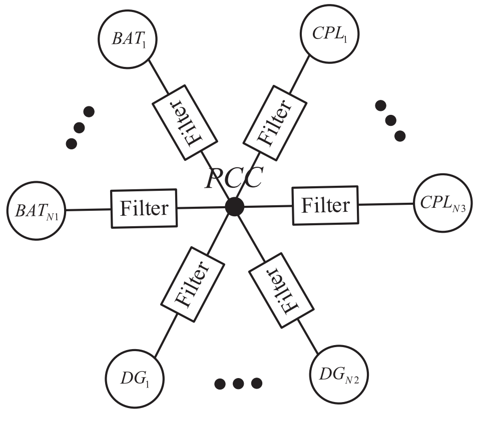

Fig. 1. Stand-alone supply systems.

The rest of this article is organized as follows. In Section II, the analysis and modeling of the stand-alone supply system are provided. Then, the impedance-based stability criteria based on the forbidden region is reviewed, and the novel stability forbidden/operation region is constituted through the rotation mapping and translation mapping in Section III. Furthermore, the stability forbidden/operation region is switched as the condition that the equivalent return-ratio matrix is Hurwitz. Moreover, The droop coefficients stability region is calculated by the proposed adaptive step search strategy in Section IV. The simulation and experimental results are separately provided to validate the performance of the proposed stability forbidden/operation criterion and the proposed adaptive step search strategy in Sections V and VI. Finally, this article is concluded in Section VII.

II. ANALYSIS AND MODELING OF THE STAND-ALONE SUPPLY SYSTEMS

The structure of the stand-alone supply system consisting of plenty of batteries, DGs and CPLs is shown in Fig. 1 [24] where the battery is named as BAT. Therein, N_1, N_2, and N_3 represent the numbers of the batteries, DGs and CPLs, respectively. Meanwhile, the battery and the DG are separately controlled by droop control strategy and P&Q control strategy [5], and the load is interfaced through the tightly regulated power electronics converter, which operates as CPL [20]. In this article, the type of DG is the renewable energy resource, such as wind energy, solar energy, and so on. Since this article focuses on small-signal stability identification, the timescale between droop controller and controller regarding the DG output is different. Based on this, the DG is always regarded as an ideal dc voltage source, which is found in the literatures [2], [25]. (As mentioned before, the renewable energy resources are simply replaced by ideal dc

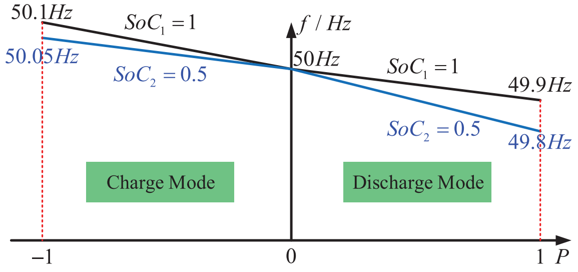

Fig. 2. Active power droop curve of the battery.

voltage sources). As a result, the renewable energy resources, which can be wind energy, solar energy, and so on, are simply replaced by ideal dc voltage sources. Furthermore, this structure will be changed accordingly to assume the presence of the number and type of the converters. The detailed analysis of this stand-alone supply system can be depicted as follows.

First, the droop functions, which are shown as 1) and 2), are widely applied to battery inverter controller. These droop functions are proposed to achieve accurate power sharing among numerous batteries without communication mode, which can improve the efficiency of renewable energy and the stability of the system. According to different demands, the SoC exponent n can be chosen. The detailed expression regarding this droop function advantage can also be found in [5]

$$f = f_0 - m_P P = f_0 - \frac{m_0}{\mathrm{SoC}^n} \times P,\ P \geq 0 \tag{1}$$

$$f = f_0 - m_P P = f_0 - m_0 \mathrm{SoC}^n \times P,\ P < 0 \tag{2}$$

where m_0 is the active power droop coefficient for $\mathrm{SoC} = 1$, and n represents the SoC exponent ($n > 0$). Although the droop control strategy provides the flexibility and reliability for power sharing, it also causes problems in stability and dynamic characteristics. For example, if the m_0 is too high, the system will be unstable, whereas if m_0 is too low, the system response speech will be reduced. Therefore, there is an important tradeoff between stability and dynamic response. For the viewpoint of SoC exponent n, on the one hand, low n causes the slope of the droop curve to vary slightly, and m_P is similar to m_0. On the other hand, high n causes the slope of the droop curve to vary dramatically, and m_P reaches higher value than m_0 for discharge mode ($P > 0$) and lower value than m_0 for charge mode ($P < 0$). For example, if $f_0 = 50$ Hz, $m_0 = 0.1$ Hz, and $n = 1$ are chosen, the active power droop curve is shown in Fig. 2. As a result, the active power droop coefficient varies with both battery SoC and charge/discharge mode. Additionally, the reactive power droop control is shown in (3). Therein, the reactive power droop coefficient of the batteries is not directly related to their SoC level and is available in light of their converters extra/unused capacity. It is worth noting that the battery with lower SoC can supply a greater number of reactive power, which reflects its higher unused converter capacity [5]

$$V = V_0 - n_Q Q. \tag{3}$$

Thus, the active and reactive droop coefficients are changing with the battery SoC and charge/discharge mode. Therefore, the stability operation region of the droop coefficients should be calculated to provide the guidance for the energy management of batteries and stabilization method research works. Since SoC value of battery and charging/discharging mode are always changed, the equivalent droop coefficient m_p is often changed for SoC-based droop control. Meanwhile, the normal droop coefficient is always a fixed value. Therefore, it is more important for power system designers to provide the stability region analysis approach for SoC-based droop control, which ensures that overcharge and overdischarge of battery will not happen. Based on this, this article will propose an SoC-based droop coefficients stability region analysis approach in Section IV. Of course, the stability regions in charging and discharging mode are different, and the SoC exponent n has also effect on the system stability. The aim of this article is to provide a generalized guidance for microgrid system operation, which ensures that overcharge and overdischarge of the battery will not happen. First, the battery is always controlled through SoC-based droop controller to balance the battery SoCs without the utilization of communications. Therein, the discharging and charging droop functions are shown as (1) and (2), respectively [5]. In order to apply the proposed approach to a random system with different SoC exponent n and charging/discharging switching mode, the stability region of the equivalent droop coefficient m_p is provided, which includes charging/discharging mode, SoC exponent n and SoC value. Therein, the SoC exponent n is chosen through power system designers, and charging and discharging mode is switched through practical power demand. Once the SoC exponent n and charging/discharging mode are set, the stability region of SoC value is provided through the proposed stability region identification approach. For example, if the battery is under discharging mode, the stability region of SoC value is $\mathrm{SoC} = (m_0/m_p)^{1/n}$, where the stability region of m_p is provided through the proposed adaptive step search strategy in Section IV. Meanwhile, the battery is under charging mode, the stability region of SoC value is $\mathrm{SoC} = (m_p/m_0)^{1/n}$, where the stability region of m_p is also provided through the proposed adaptive step search strategy in Section IV. To sum up, the SoC characteristics, such as charging/discharging mode and SoC exponent n, have been embedded into the proposed stability region identification approach. The equivalent droop coefficient is defined in this article to make the stability region identification approach more widely applicable.

In light of the impedance approach, the stand-alone supply system is stable if and only if the two conditions are satisfied at the same time, i.e., subsystem stability and interactive stability. On one hand, each subsystem stability can be identified via the state-space approach, and the interactive stability among each subsystem can be identified via impedance approach [20]. Obviously, the fluctuation of the droop coefficients results in both subsystem and interactive instability. First and foremost, the battery subsystem stability is widely studied, and the complete state-space model of the ith battery is established as follows:

$$x_i = \begin{bmatrix} \Delta\delta_i & \Delta P_i & \Delta Q_i & \Delta\phi_{di} & \Delta\phi_{qi} \\ \Delta\gamma_{di} & \Delta\gamma_{qi} & \Delta i_{ldi} & \Delta i_{lqi} & \Delta i_{0di} \\ \Delta i_{0qi} & \Delta v_{0di} & \Delta v_{0qi} & & \end{bmatrix}^T_{13\times 1}. \tag{4}$$

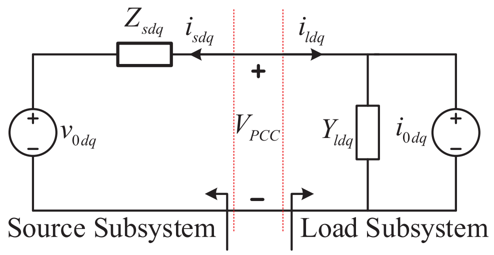

Fig. 3. Interconnection of two stable independent systems.

The detailed state-space model is obtained in [10], and the state matrix of the ith battery is defined as A_i. Moreover, the subsystem stability of the ith battery is ensured if and only if A_i is Hurwitz. In this article, each CPL is stable when supplied by an ideal voltage source, and each P&Q controlled inverter is stable when connected to the utility grid. If each subsystem is stable, the stand-alone supply system shown in Fig. 1 is divided into source subsystem and load subsystem, which is expressed in Fig. 3. The stand-alone supply system is stable if and only if the Nyquist contour of the return-ratio matrix (R) does not encircle the $(-1, j0)$ point [20]. Therein, these batteries belong to the source subsystem, and DGs and CPLs belong to the load subsystem. First, the output impedance matrix of the ith droop-controlled battery is provided in [26], and it is defined as Z_i. Considering the stand-alone supply system with multiple batteries, the output impedance matrix is calculated as follows: $Z_{\mathrm{sdq}} = Z_1//Z_2//\ldots//Z_{N1}$ [24]. Second, the input admittance matrix of the ith P&Q controlled DG is provided in [27], and it is defined as Y_{invi}. Likewise, the input admittance matrix of multiply DGs is calculated as follows: $Y_{\mathrm{inv}} = Y_{\mathrm{inv1}}//Y_{\mathrm{inv2}}//\ldots//Y_{\mathrm{inv}N2}$ [24]. Third, the input admittance matrix of the ith CPL is provided in [28], and it is defined as $Y_{\mathrm{CPL}i}$. Meanwhile, the input admittance matrix of multiply CPLs is calculated as follows: $Y_{\mathrm{CPL}} = Y_{\mathrm{CPL1}}//Y_{\mathrm{CPL2}}//\ldots//Y_{\mathrm{CPL}N3}$ [24]. As a result, the total input admittance matrix of the stand-alone supply system is $Y_{\mathrm{ldq}} = Y_{\mathrm{inv}}//Y_{\mathrm{CPL}}$. Eventually, the return-ratio matrix of the stand-alone supply system is expressed as follows:

$$R = Z_{\mathrm{sdq}} Y_{\mathrm{ldq}}. \tag{5}$$

III. STABILITY FORBIDDEN/OPERATION REGION CRITERION BASED ON RETURN-RATIO MATRIX

Assuming that each subsystem is stable, the stand-alone supply system is stable if and only if the $E + Z_{\mathrm{sdq}}Y_{\mathrm{ldq}}$ does not have the right pole, where E is a 2×2 unit matrix [20], [28]. In other words, the necessary and sufficient condition for stability of the stand-alone supply system is obtained that the Nyquist contour of the return-ratio matrix ($R = Z_{\mathrm{sdq}}Y_{\mathrm{ldq}}$) does not encircle the $(-1, j0)$ point. However, the GNC is complex, and it is not suitable for the design of the ac system [20]. According to this concept, the system stability is guaranteed by maintaining the eigenvalues (λ_{Ri}, $i =$ 1,2) of the return-ratio matrix outside the certain forbidden regions. Thus, several simplified stability criteria have been proposed [20], [21], [23], i.e., forbidden region criteria and norm-based impedance criteria. Therein, there are four common forbidden region criteria, such as Middlebrook criterion, opposing argument criterion, and gain margin and phase margin (GMPM) criterion [21] and N-FRB criterion [23], which is shown in Fig. 4(a)–(d). To the best of authors' knowledge, the N-FRB criterion should have lowest conservatism among forbidden-region-based stability criteria. Although these criteria can eliminate the tedious drawing process of the generalized Nyquist curve, partial cirteria have high conservatism and N-FRB criterion is not suitable for stability region identification based on the following adaptive step search strategy in Section IV. Meanwhile, the N-FRB criterion is difficult for scholars to provide relative stability margin, such as phase margin, gain margin, and σ margin. Based on this, a novel forbidden region criterion, which is located in the left of the gray boundary in Fig. 5, for λ_{Ri} is constructed. The detailed forbidden region proposed in this article is presented in the following equation:

$$|\arg(\lambda_{Ri} + \varepsilon_{\mathrm{GM1}})| \leq 180^\circ - \theta_{\mathrm{PM}} \tag{6}$$

$$\mathrm{Re}\,(\lambda_{Ri}) \geq -\varepsilon_{\mathrm{GM2}}. \tag{7}$$

Through maintaining λ_{Ri} out of the proposed stability forbidden region, the system stability is ensured with phase margin (θ_{PM}), first gain margin ($\varepsilon_{\mathrm{GM1}}$), and second gain margin ($\varepsilon_{\mathrm{GM2}}$). Therein, it is advisable that $\theta_{\mathrm{PM}} = 60^0$, $\varepsilon_{\mathrm{GM1}} = 0$, and $\varepsilon_{\mathrm{GM2}} = 0.5$ [21]. Traditionally, the conservative stability criterion is to obtain the analytical condition, such as phase margin, gain margin, and σ margin [2]. In this article, the novel stability forbidden/operation region criterion is based on these three margins. For the proposed criterion in this article, which is shown in Fig. 4(e), the phase margin, gain margin, and σ margin in the proposed criterion are θ_{PM}, $\varepsilon_{\mathrm{GM1}}$, and $\varepsilon_{\mathrm{GM2}}$, respectively. It is worth noting that the smaller the area of the stability forbidden region is, the less conservative the criterion is. Four common forbidden region criteria and the proposed criterion in this article are shown in Fig. 4 where the gray area represents the stability forbidden region. In conclusion, compared with the first three forbidden region criteria, such as middle criterion, opposing argument, and GMPM criterion, the proposed forbidden region criterion based on the eigenvalues of the return-ratio matrix is less conservative. Moreover, in essence, the norm-based impedance criteria are based on Middlebrook forbidden region criterion. And the conservatism of the norm-based impedance criteria is not lower than that of Middlebrook criterion [20]. The smaller the stability forbidden region is, the less conservative the criterion is. As a result, the proposed forbidden region criterion has less conservatism than Middlebrook criterion. Based on this, the proposed forbidden region criterion has less conservatism than the existing three norm-based stability criteria (G-norm criterion, infinity-norm criterion, and the infinity-one-norm criterion) and the partial stability forbidden region criteria (Middlebrook criterion, opposing argument criterion, GMPM criterion). Furthermore, when $\varepsilon_{\mathrm{GM1}}$ and $\varepsilon_{\mathrm{GM2}}$ tend to 1 and θ_{PM} tends to 0^0, the forbidden region proposed in this article is also decreased as one radial line $[-1, -\infty]$ on the imaginary axis. Under this case, the conservatism of this article is similar with the conservatism of the novel forbidden-region-based criterion proposed in the

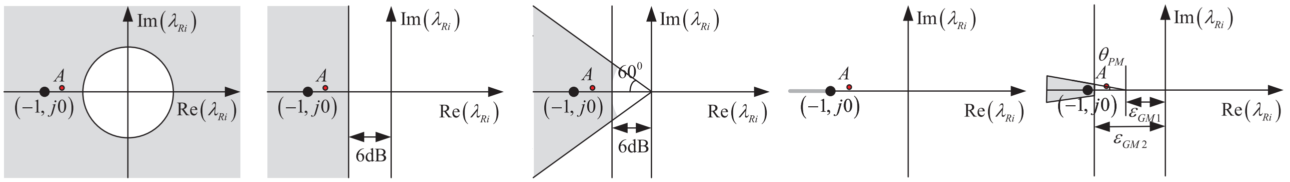

(a) (b) (c) (d) (e)

Fig. 4. Five forbidden region criteria. (a) Middlebrook Criterion. (b) Opposing Argument Criterion. (c) GMPM Criterion. (d) N-FRB Criterion. (e) Proposed Criterion.

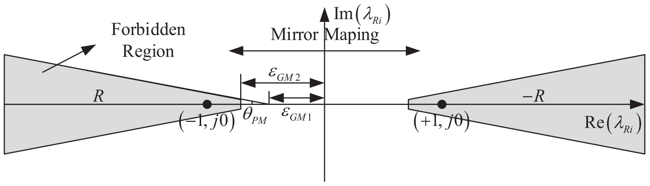

Fig. 5. Novel stability forbidden region criterion.

literature [23]. However, from the viewpoint of the stability forbidden region criteria, the generalized Nyquist curves still need to be drawn without other mathematical transformation. Therefore, the proposed stability forbidden region criterion is further switched to the Hurwitz identification criterion. First, the stability forbidden region criterion is switched to the condition that the Nyquist contour of the $-R$ does not encircle the $(1, j0)$ point, where $-R$ represents the mirror mapping matrix of the return-ratio matrix (R). Therein, the detailed proof process is described as follows.

Theorem 1: The Nyquist contour of the R does not encircle the $(-1, j0)$ point if and only if the Nyquist contour of the $-R$ does not encircle the $(1, j0)$ point.

Proof: R and $-R$ are separately reduced to the matrices in Jordan canonical form, which are shown in the following equation:

$$R = \Gamma^T \begin{bmatrix} \lambda_{R1} & 0 \\ * & \lambda_{R2} \end{bmatrix} \Gamma \tag{8}$$

$$-R = \Gamma^T \begin{bmatrix} -\lambda_{R1} & 0 \\ * & -\lambda_{R2} \end{bmatrix} \Gamma \tag{9}$$

where Γ and $*$ represent unitary matrix and arbitrary constant, respectively. If the Nyquist contour of the $-R$ does not encircle the $(1, j0)$ point, the characteristic roots $-\lambda_{R1}$ and $-\lambda_{R2}$ do not encircle the $(1, j0)$ point under arbitrary frequencies. Since $-\lambda_{R1}$ and λ_{R1} are mirror symmetric about the y-axis, the characteristic root λ_{R1} does not encircle the $(-1, j0)$ point under arbitrary frequencies. Similarly, since $-\lambda_{R2}$ and λ_{R2} are mirror symmetric about the y-axis, the characteristic root λ_{R2} does not encircle the $(-1, j0)$ point under arbitrary frequencies. Therefore, if the Nyquist contour of the $-R$ does not encircle the $(1, j0)$ point, the Nyquist contour of the R does not encircle the $(-1, j0)$ point. In the same way, if the Nyquist contour of the R does not encircle the $(-1, j0)$ point, the Nyquist contour of the $-R$ does not encircle the $(1, j0)$ point. As a result, the Nyquist contour of the R does not encircle the $(-1, j0)$ point if and only if the Nyquist contour of the $-R$ does not encircle the $(1, j0)$ point.

In summary, the return-ratio matrix stability operation region is constructed through $-R$. What is more, the proposed stability operation region includes three subregions, e.g., A_{R1}, A_{R2}, and A_{R3}. A_{R1} is constructed through translation mapping. Both A_{R2} and A_{R3} are constructed through translation mapping and rotation mapping. The detailed stability operation subregions are expressed in Fig. 6. Finally, these three subregions can be provided as follows, where, R_1, R_2, and R_3 are Hurwitz:

$$A_{R1}: \quad R_1 = -R - \varepsilon_{\text{GM2}} E \tag{10}$$

$$A_{R2}: \quad R_2 = -\left(R + \varepsilon_{\text{GM1}} E\right) \times e^{j(\pi/2 - \theta_{\text{PM}})} \tag{11}$$

$$A_{R3}: \quad R_3 = -\left(R + \varepsilon_{\text{GM1}} E\right) \times e^{-j(\pi/2 - \theta_{\text{PM}})}. \tag{12}$$

R_1, R_2, and R_3 are defined as the equivalent return-ratio matrices, which are the parameter-dependent nonlinear time-invariant matrices under Laplace transformation. To sum up, the interactive stability forbidden/operation region criterion based on return-ratio matrix is switched to the Hurwitz matrix identification criterion.

Remark 1: The detailed switching process can be written as follows. First, if each subsystem is stable, the stand-alone supply system is stable if and only if the Nyquist contour of the return-ratio matrix (R) does not encircle the $(-1, j0)$ point [20]. Second, according to Theorem 1, the stability identification condition can be switched as the condition that the Nyquist contour of the return-ratio matrix ($-R$) does not encircle the $(1, j0)$ point. Third, if the characteristic roots $-\lambda_{R1}$ and $-\lambda_{R2}$ are located into the green region, which are shown in Fig. 6, the Nyquist contour of the return-ratio matrix ($-R$) must not encircle the $(1, j0)$ point. Fourth, these three subregions can be switched into left half-plane through translation mapping and rotation mapping. Undoubtedly, the characteristic roots of one matrix are located into left half-plane if and only if this matrix is Hurwitz. Based on this, the stability subregion is switched as Hurwitz matrix space through relative mapping.

IV. ADAPTIVE STEP SEARCH STRATEGY BASED ON GENERALIZED INCIDENCE MATRIX

According to the foresaid section, the stability of the stand-alone supply system is guaranteed if both subsystem stability and interactive stability are satisfied at the same time. Therefore, the generalized incidence matrix, combining state-steady function of the subsystem and stability operation region criterion of the interactive system, is first constructed in this article as follows:

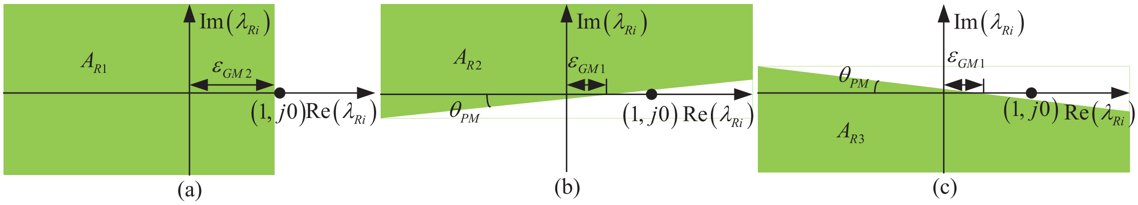

Fig. 6. Stability operation subregions. (a) Stability subregion A_{R1}. (b) Stability subregion A_{R2}. (c) Stability subregion A_{R3}.

$R_{Gi} = \mathrm{diag}(A_1, A_2, \ldots A_N, R_i)$, where $i = 1, 2$, and 3. To sum up, the stability of the stand-alone supply system consisting of multiply batteries is guaranteed if at least one of these three generalized incidence matrices is Hurwitz.

In order to calculate the droop coefficients stability region considering multiply batteries, the generalized incidence matrix should be built in polar coordinates. Given one vector $(m_{P1}, n_{Q1}, m_{P2}, n_{Q2}, \ldots, m_{Pk}, n_{Qk}) \in R^{2\,k}, k \geq 1$, there exists one real number r and $2k - 1$ scalars $\delta_i \in [0, \pi), i = 1, 2, \ldots, 2\,k$ such that $(m_{P1}, n_{Q1}, m_{P2}, n_{Q2}, \ldots, m_{Pk}, n_{Qk})^T = rf(\delta)$. Therein, $\delta \triangleq (\delta_2, \delta_3, \ldots, \delta_{2\,k})^T \in [0, \pi)^{2\,k-1}$, and $f(\delta) \triangleq (\cos\delta_2, \sin\delta_2\cos\delta_3, \ldots, \sin\delta_2\sin\delta_3 \ldots \sin\delta_{2\,k}) \in [-1, 1]^{2\,k}$ [29]. Meanwhile, the δ_i is selected as an universal set ($\delta_i = [0^0, 1^0, \ldots, 180^0]$). Once δ is determined, the multivariable parameter-dependent nonlinear time-invariant matrix is switched to the single-variable parameter-dependent nonlinear time-invariant matrix. Likewise, the generalized incidence matrix is also a transfer function matrix, which is transformed into the Euclidean space matrix under a series of discrete frequencies. Thereinto, the frequencies set is always selected as an universal set ($f_{\mathrm{tab}} = [f_1, f_2, \ldots, f_i, \ldots, f_n]Hz = [1, 2, \ldots, 20\,000]$Hz). In conclusion, the adaptive step search strategy based on the generalized incidence matrix will be designed to obtain the droop coefficients stability region. In order to enhance the adaptability of the algorithm, the least mean square is applied to regard as growth factor, which is expressed as follows:

$$r\,(m+1) = r(m) + \mathrm{sign}(L_{\min}) \times \Delta r(0) \times |L_{\min}|^{\lambda(m)} \tag{13}$$

$$\lambda(m) = \alpha \times \left(1 + e^{-\beta|s(m)|^2}\right) \tag{14}$$

$$s(m) = \gamma s\,(m-1) + (1-\gamma)\,L_{\min} \tag{15}$$

where $\mathrm{sign}(x)$ represents sign function. $L_{\min}$ represents the minimum eigenvalue real part of the generalized incidence matrices. $|L_{\min}|^{\lambda(m)}$ and $\lambda(m)$ represent variable step coefficient and step growth factor, respectively. Both α and β represent adjustment factors. γ represents forgetting factor. Thus, the detailed calculation steps are follows.

Step 1: Initialize global variable, i.e., $r(0) = 0$, $m = 0$, and $\Delta r(0) = 0$.

Step 2: Initialize partial variable, i.e., $L_{\max1} = \emptyset$, $L_{\max2} = \emptyset$, $L_{\max3} = \emptyset$, and $i = 1$.

Step 3: Calculate the return-ratio matrix ($R(s)$) of the stand-alone supply system, where $s = -j2\pi f_i$. Under this frequency, the three generalized incidence matrices (R_1, R_2, and R_3) are calculated, respectively.

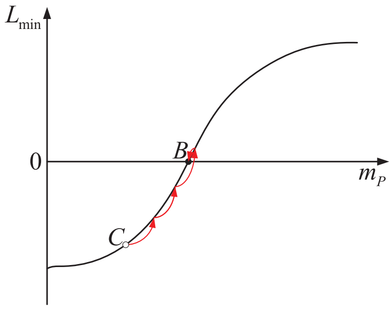

Fig. 7. Relationship between $L_{\min}$ and m_P.

Step 4: Calculate the maximum real part values among the λ_{R1}, λ_{R2}, and λ_{R3}, i.e., $L_1 = \max(\mathrm{real}(\mathrm{eig}(R_1)))$, $L_2 = \max(\mathrm{real}(\mathrm{eig}(R_2)))$, and $L_3 = \max(\mathrm{real}(\mathrm{eig}(R_3)))$.

Step 5: Expand matrices, i.e., $L_{\max1} = [L_{\max1}, L_1]$, $L_{\max2} = [L_{\max2}, L_2]$, and $L_{\max3} = [L_{\max3}, L_3]$. If $i < 20\,000$, $i = i + 1$, then go to *Step 3*. Else, go to *Step 6*.

Step 6: Select the maximum values among the $L_{\max1}$, $L_{\max2}$, and $L_{\max3}$, i.e., $L_{\max-1} = \max(L_{\max1})$, $L_{\max-2} = \max(L_{\max2})$, and $L_{\max-3} = \max(L_{\max3})$. Define that $L_{\min}$ is the minimum value among $L_{\max-1}$, $L_{\max-2}$, and $L_{\max-3}$, i.e., $L_{\min} = \min(L_{\max-2}, L_{\max-1}, L_{\max-3})$.

Step 7: Determine if $L_{\min}$ is zero for $r(m)$. If yes, keep a record of such open interval in $(0, r(m))$, and go to *Step 8*. If no, $r(m+1) = r(m) + \mathrm{sign}(L_{\min}) \times \Delta r(0) \times |L_{\min}|^{\lambda(m)}$, then go to *Step 2*.

Step 8: Calculate the union of all the open intervals recorded in *Step 7*, and the recorded result is the stability region while δ sets one certain value. If the vector δ has applied all the values in $[0, 2\pi)^{2\,k-1}$, the final stability region of the stand-alone supply system is obtained. If no, go to *Step 1*.

The stability region identification problem is transformed into Hurwitz identification problem through the proposed stability criterion and relative mapping. In order to obtain the droop coefficient stability region, the adaptive step search strategy is proposed in this article. As shown in [30], with the increase of droop coefficient, the stability margin of the system will be decreased. Thus, the relationship between $L_{\min}$ and m_P is shown in Fig. 7 where red line represents the movement locus based on the proposed adaptive step search strategy. There is no doubt that the proposed adaptive step search strategy is based on the bisection method. Therein, the bisection method is an initial independent convergence algorithm. Thus, the stability/convergence of the

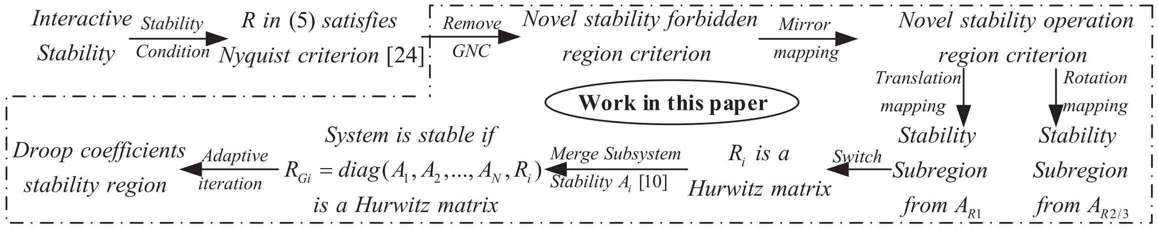

Fig. 8. Switching process from stability region identification to Hurwitz identification.

adaptive step search strategy can be ensured, and similar concept has been applied to the adaptive perturbation observation method to achieve maximum power tracking in the wind/solar system.

According to the foresaid discussion, the stand-alone supply system is stable if both subsystem stability and interactive stability can be satisfied at the same time [26]. From the viewpoint of subsystem stability, it can be identified through state-space function [10]. The ith battery is stable if and only if the state function A_i is Hurwitz. Meanwhile, interactive stability can be satisfied if and only if the return-ratio matrix R satisfies NC, which is based on the impedance approach [26]. In order to eliminate complex Nyquist drawn process and provide relative preprocessing, the novel stability forbidden region criterion has been proposed, which is further switched into stability operation region criterion. Moreover, the stability region is divided into three stability subregion. The stability subregion is first switched as Hurwitz matrix space through the rotation mapping and translation mapping. As a result, the stability region criterion regarding interactive stability is transformed into the Hurwitz identification problem through mirror, rotation and translation mapping, which is found in Section III. Eventually, the subsystem and interactive stability can be combined, i.e., $R_{Gi} = \mathrm{diag}(A_1, A_2, \ldots A_N, R_i)$, where $i = 1, 2,$ and 3. The stand-alone supply system is stable if one of the generalized incidence matrices R_{Gi} is Hurwitz. The foresaid illustrations are shown in Fig. 8.

V. SIMULATION RESULTS

In order to verify the performance of the proposed droop coefficients stability region analysis approach based on the generalized incidence matrix, the two series simulation testing systems shown in Fig. 1, are provided as follows: conservatism verification and effectiveness verification. The detailed parameters are listed in Table I. In this section, these regulated power electronics converters loads and P&Q controlled inverters are stable when connected to an ideal voltage source [26], [27]. Meanwhile, the structure of the stand-alone supply system is changed accordingly to assume the presence of the numbers of these batteries, DGs and CPLs. In order to reduce the conservatism of the proposed stability forbidden/operation region criterion, the phase margin and gain margins are set that $\theta_{\mathrm{PM}} = 5^0$, $\varepsilon_{\mathrm{GM1}} = 0.95$, and $\varepsilon_{\mathrm{GM2}} = 0.99$.

Remark 2: According to the literature [31], if the system is stable but very close to critical stable, even the little change of parameters will make the system unstable. To this end, stability margin is an indispensable consideration factor for one stable system to enhance the system's relative stability. Traditionally, the conservative stability criterion is to obtain the analytical condition, such as phase margin, gain margin, and σ margin [2]. In order to ensure the system stability under parameters perturbation, it is advisable that $\theta_{\mathrm{PM}} = 60^0$, $\varepsilon_{\mathrm{GM1}} = 0$, and $\varepsilon_{\mathrm{GM2}} = 0.5$ [21]. There is no doubt that the proposed stability criterion will have high conservatism. There is a tradeoff between stability margin and conservatism. Therein, the aim of this article is to obtain SoC-based droop coefficients stability region, which is advisable for power designers to obtain more accurate region. Therefore, the relative margin should be chosen as minimum values. Of course, if scholars want to obtain one parameter stability region with robustness, θ_{PM}, $\varepsilon_{\mathrm{GM1}}$, and $\varepsilon_{\mathrm{GM2}}$ can be chosen as $\theta_{\mathrm{PM}} = 60^0$, $\varepsilon_{\mathrm{GM1}} = 0$, and $\varepsilon_{\mathrm{GM2}} = 0.5$.

TABLE I
SIMULATION AND EXPERIMENTAL TESTING SYSTEM PARAMETERS

Detailed parameters of the droop controlled inverter			
Voltage controller	$G_v = 1 + 8/s$	Filter inductor	$6mH$
Current controller	$G_c = 4 + 150/s$	Filter capacitor	$600\mu F$
Detailed parameters of the $P\&Q$ controlled inverter			
Power controller	$G_p = 0.5 + 40/s$	Filter capacitor	$50\mu F$
Current controller	$G_c = 0.3 + 10/s$	Filter inductor	$5mH$
Phase-locked loop	$G_{PLL} = 0.58 + 10/s$	Low pass filter	$5Hz$
Detailed parameters of the regulated power electronic converter load (CPL)			
Voltage controller	$G_v = 0.4 + 4/s$	Filter inductor	$1mH$
Current controller	$G_c = 3 + 100/s$	Filter resistor	$0.1m\Omega$
Phase-locked loop	$G_{PLL} = 0.58 + 10/s$	Bus capacitor	$20mF$

A. Conservatism Verification

In this section, the comparison among the stability forbidden region criteria, norm-based impedance criteria, and the proposed stability forbidden/operation region criteria is provided to verify that the proposed criterion is less conservative. First and foremost, the number of both the droop controlled inverter and the CPL is one, and the number of the P&Q controlled inverter in the stand-alone supply system is zero. The active/reactive power droop coefficients are chosen as follows: $m_P = 2 \times 10^{-4}$ and $n_Q = 3.4 \times 10^{-3}$. And the capacity of the CPL is 18 kW. According to the literature [2], the droop controlled inverter is stable when unloading, i.e., when the load is an open circuit. Based on this, the reason that the stand-alone supply system is unstable, is interactive instability between the source subsystem and load subsystem. According to the parameters in Table I, the return-ratio matrix of the stand-alone supply system is shown as

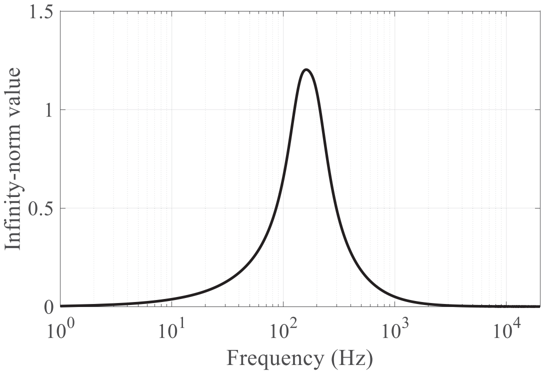

Fig. 9. Infinity-norm impedance criterion.

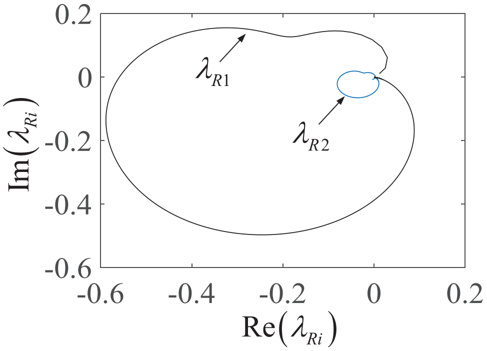

Fig. 10. Generalized Nyquist curve at the initial moment.

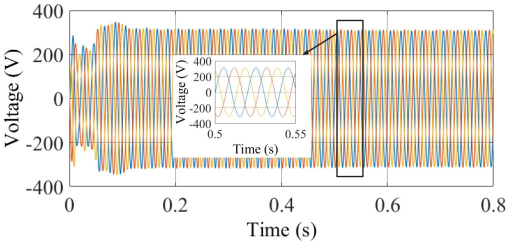

Fig. 11. Initial three-phase voltage waveform of the ac bus in Section V-A.

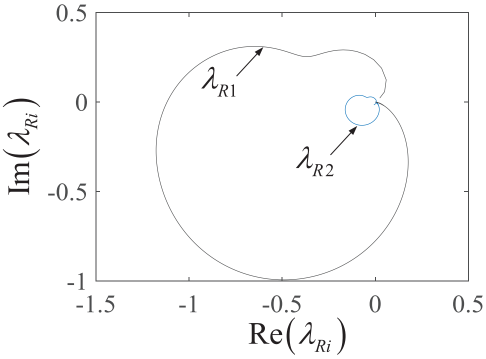

Fig. 12. Generalized Nyquist curve under changed load.

follows:

$$R = \begin{bmatrix} -0.8134 + j0.0394 & -0.0207 - j0.0113 \\ 0.3552 + j0.1220 & -0.0501 + j0.0044 \end{bmatrix}. \tag{16}$$

Therefore, the two eigenvalues of the return-ratio matrix are $-0.8060 + j0.0485$ and $-0.0575 - j0.0047$, respectively. For the first three forbidden stability region criteria, the eigenvalue with smaller negative real part is regarded as point A in Fig. 4(a) and (c), in which the point A is located in the forbidden region. According to three forbidden region criteria, it is possible that the stand-alone supply system is unstable. Furthermore, the infinity-norm impedance criterion has lower conservatism among three norm-based impedance criteria, and the infinity-norm value of the return-ratio matrix is larger than unit if system frequency belongs to the interval $[126\text{ Hz}, 212\text{ Hz}]$, which is shown in Fig. 9. Thus, it is possible that the stand-alone supply system is unstable. However, the eigenvalue with smaller negative real part is regarded as point A in Fig. 4(d)–(e), in which the point A is outside the forbidden region based on N-FRB criterion and the proposed criterion. According to N-FRB criterion or the proposed stability forbidden criterion, the stand-alone supply system must be stable. Moreover, the first generalized incidence matrix, which is proposed in this article, is also Hurwitz in the interval $[0\text{ Hz}, 20\,000\text{ Hz}]$. As a result, the stand-alone supply system must be stable. It is convenient to compare the conservatism results among the proposed criterion, the forbidden region criteria and norm-based impedance criteria through the time-domain voltage waveform and GNC. As shown in Fig. 10, the Nyquist contour of the return-ratio matrix ($R = Z_{\mathrm{sdq}} Y_{\mathrm{ldq}}$) does not encircle the $(-1, j0)$ point, and the stand-alone supply system must be stable. Meanwhile, as shown in Fig. 11, the voltage of the ac bus in the stand-alone supply system is stable. Based on the foresaid simulation results, the proposed stability forbidden/operation region criterion has lower conservatism than the existing partial stability forbidden region criteria and norm-based impedance criteria. Meanwhile, the proposed stability forbidden/operation region criterion has similar conservatism with N-FRB criterion.

Furthermore, in order to illustrate the impact of load change, the number of CPLs is changed as two, and the total power of CPL is 36 kW. Thus, the return-ratio matrix of the standalone supply system is shown as follows:

$$R = 2 \times \begin{bmatrix} -0.8134 + j0.0394 & -0.0207 - j0.0113 \\ 0.3552 + j0.1220 & -0.0501 + j0.0044 \end{bmatrix}. \tag{17}$$

Under this case, none of these generalized incidence matrices is the Hurwitz matrix. As a result, it is possible that this system is unstable. As shown in Fig. 12, the Nyquist contour of the return-ratio matrix ($R = Z_{\mathrm{sdq}} Y_{\mathrm{ldq}}$) encircles the $(-1, j0)$ point, and the stand-alone supply system must be unstable. Meanwhile, as shown in Fig. 13, the voltage of the ac bus in the stand-alone supply system is unstable. Therefore, with the increasing of CPL, the system stability margin is decreased, and this phenomenon has also been reported in previous research works [20].

B. Effectiveness Verification

In order to better verify the effectiveness of the proposed stability region identification approach, the simulation results in this section are divided into two aspects, i.e., source subsystem

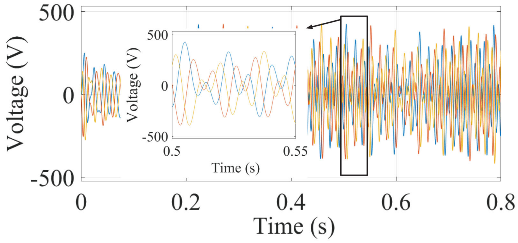

Fig. 13. Three-phase voltage waveform of the ac bus under changed load in Section V-A.

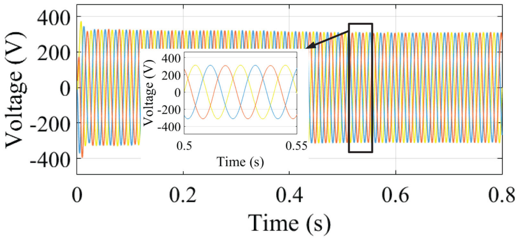

Fig. 14. Three-phase voltage simulation waveform under $m_{P1} = 2 \times 10^{-4}$ and $n_{Q1} = 3.4 \times 10^{-3}$.

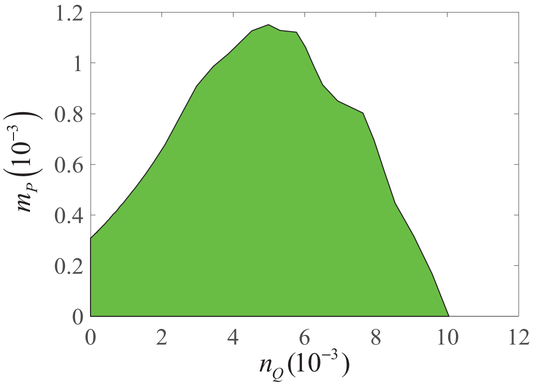

Fig. 15. Droop coefficients stability region.

change (battery capacity change, SoC exponent change, and SoC change) and load subsystem change (rated DG capacity change and CPL change). Therein, the number of both the P&Q controlled inverters and the droop controlled inverters is two, and the number of the CPLs in the stand-alone supply system is three. Meanwhile, the rated capacities of the first CPL, the second CPL, and the third CPL are 18, 9, and 9 kW, respectively. And the rated capacity of each DG is 10 kW. The other parameters are found in Table I. Under this case, the stand-alone supply system is stable, and three-phase voltage waveform is shown in Fig. 14. Assuming that the active/reactive droop coefficients of the second battery are unchanged, the stability region regarding active/reactive droop coefficients of the first battery is obtained to verify the performance of the proposed adaptive step search strategy. According to the proposed adaptive step search strategy, the stability boundary radius under different δ is provided in Table II. Therein, the $m_P = R\cos(\delta\pi/180)/1000$ and $n_Q = R\sin(\delta\pi/180)/1000$. Thus, the stability region, which is shown in Fig. 15, can be obtained through MATLAB.

TABLE II
DROOP COEFFICIENTS STABILITY REGION BASED ON THE PROPOSED ADAPTIVE STEP SEARCH STRATEGY

δ	R	δ	R	δ	R	δ	R	δ	R
1	0.309	2	0.309	3	0.310	4	0.311	5	0.313
6	0.314	7	0.316	8	0.317	9	0.319	10	0.321
11	0.323	12	0.325	13	0.327	14	0.329	15	0.331
16	0.334	17	0.336	18	0.339	19	0.342	20	0.346
21	0.348	22	0.352	23	0.356	24	0.359	25	0.363
26	0.368	27	0.372	28	0.377	29	0.379	30	0.387
31	0.393	32	0.398	33	0.405	34	0.410	35	0.417
36	0.424	37	0.432	38	0.439	39	0.448	40	0.456
41	0.465	42	0.475	43	0.486	44	0.496	45	0.509
46	0.519	47	0.532	48	0.547	49	0.562	50	0.578
51	0.597	52	0.614	53	0.634	54	0.654	55	0.681
56	0.704	57	0.734	58	0.764	59	0.794	60	0.829
61	0.869	62	0.919	63	0.969	64	1.020	65	1.091
66	1.165	67	1.255	68	1.355	69	1.485	70	1.645
71	1.865	72	2.19	73	3.11	74	3.58	75	4.01
76	4.66	77	5.12	78	5.43	79	5.88	80	6.12
81	6.33	82	6.57	83	6.98	84	7.68	85	7.98
86	8.25	87	8.55	88	9.07	89	9.58	90	10.049

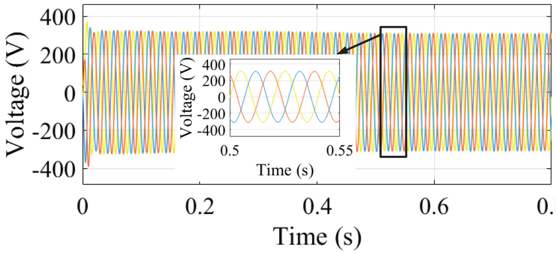

Fig. 16. Three-phase voltage simulation waveform under $m_{P1} = 5 \times 10^{-4}$ and $n_{Q1} = 3.4 \times 10^{-3}$.

First, the proposed stability region identification approach is verified under source subsystem change. The battery characteristics, such as SoC value, SoC exponent, and battery capacity, have been embedded into the equivalent droop coefficient. Under discharging mode, the equivalent droop coefficient $m_p = m_0/\mathrm{SoC}^n$, and under charging mode, the equivalent droop coefficient $m_p = m_0\mathrm{SoC}^n$. Therein, m_0 is inversely proportional to the battery capacity. At the initial moment, the droop coefficients of the first battery are $m_{P1} = 5 \times 10^{-4}$ and $n_{Q1} = 3.4 \times 10^{-3}$. Under this case, the droop coefficients point is located in the green area of Fig. 15, which illustrates that the stand-alone supply system must be stable. The three-phase voltage is stable, which is shown in Fig. 16. Therein, the simulation result is in accordance with the conclusion of the proposed adaptive step search strategy. Since the aim of this article is to ensure that overcharge and overdischarge of battery will not happen, the following three cases should be considered to verify the effectiveness of the proposed stability region identification approach.

1) The SoC value of battery is decreased under discharging mode or increased under charging mode.
2) The SoC exponent of battery is decreased under discharging mode or increased under charging mode.
3) The battery capacity is decreased, which represents m_0 is increased.

In order to verify the performance of the proposed stability region identification approach, one of the three cases is chosen, which are shown as follows.

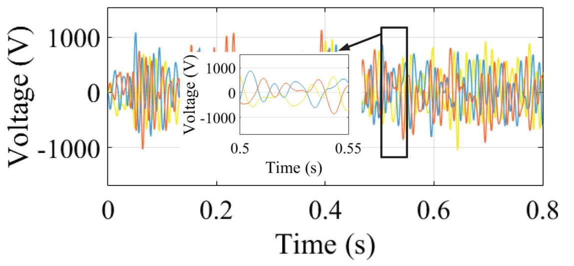

Fig. 17. Three-phase voltage simulation waveform under $m_{P1} = 2 \times 10^{-3}$ and $n_{Q1} = 3.4 \times 10^{-2}$.

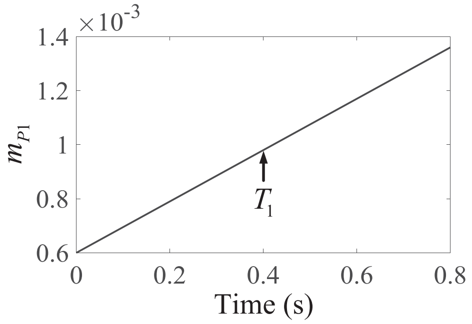

Fig. 18. Variation curve regarding droop coefficient in simulation.

1) The SoC value of the first battery is reduced to a quarter under discharging mode or enlarged by four times under charging mode.
2) Both SoC value and SoC exponent of the first battery are cut to half under discharging mode or enlarged by two times under charging mode.
3) The first battery capacity is reduced to a quarter under both discharging mode and charging mode.

Based on this, the equivalent droop coefficients of the first battery are changed as $m_{P1} = 2 \times 10^{-3}$ and $n_{Q1} = 3.4 \times 10^{-2}$. As a result, the droop coefficients point is outside stability region, and it is possible that the stand-alone supply system is unstable. As shown in Fig. 17, the instability phenomenon has occurred in the stand-alone supply system. Furthermore, the reactive droop coefficient is chosen as $n_{Q1} = 3.4 \times 10^{-3}$. Meanwhile, the active droop coefficient m_{P1} is variable, and its change is based on Fig. 18. Before T_1, droop coefficients point is located into stability region, which is shown in Fig. 15, and the stand-alone supply system must be stable. Furthermore, after T_1, droop coefficients point is outside stability region. Under this case, it is possible that the stand-alone supply system is unstable. As shown in Fig. 19, three-phase voltage simulation waveform is in accordance with the proposed stability region identification strategy. As a result, the effectiveness of the proposed adaptive step search strategy based on generalized incidence matrix is ensured through simulation results.

Second, the proposed stability region identification approach is verified under load subsystem change. Since the discussion of the load changed case has been provided in Section V-A, the different ratings of DG are discussed in this section. The total rating of DG is changed from 20 to 30 kW. Under this case, the droop coefficients stability region based on the proposed adaptive step search strategy is shown in Fig. 20 where the stability region is green area. There is no doubt that the droop coefficients stability region is reduced through improving penetration of renewable energy. This phenomenon has also been found in the previous research works [32]. First of all, the droop coefficients of the first battery are $m_{P1} = 8 \times 10^{-4}$ and $n_{Q1} = 3.4 \times 10^{-3}$. Under this case, the droop coefficients point is located in green area of Fig. 20, which illustrates that the stand-alone supply system must be stable. As shown in Fig. 21, the three-phase voltage is stable. Furthermore, the droop coefficients of the first battery are changed as $m_{P1} = 1.2 \times 10^{-3}$ and $n_{Q1} = 3.4 \times 10^{-3}$. Under this case, the droop coefficients point is outside stability region. As a result, it is possible that the stand-alone supply system is unstable. As shown in Fig. 22, the instability phenomenon has occurred in the stand-alone supply system. Thus, the performance of the proposed approach can be verified.

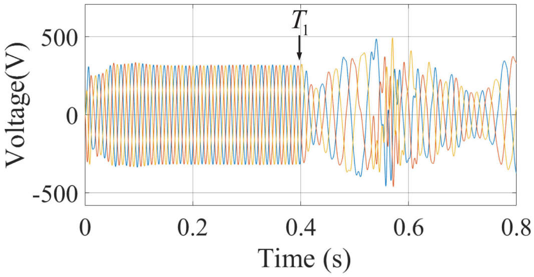

Fig. 19. Three-phase voltage simulation waveform under variable droop coefficients.

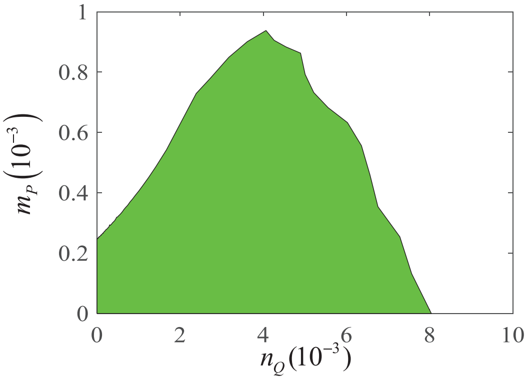

Fig. 20. Droop coefficients stability region under load subsystem change.

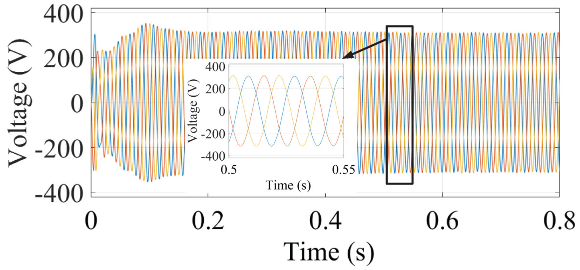

Fig. 21. Three-phase voltage simulation waveform under $m_{P1} = 8 \times 10^{-4}$ and $n_{Q1} = 3.4 \times 10^{-3}$.

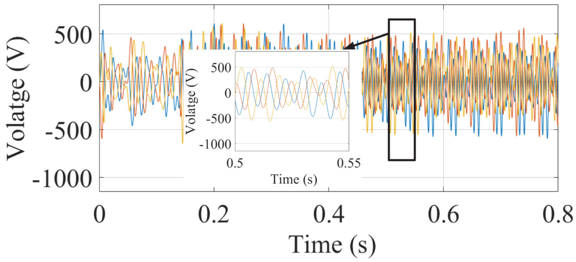

Fig. 22. Three-phase voltage simulation waveform under $m_{P1} = 1.2 \times 10^{-3}$ and $n_{Q1} = 3.4 \times 10^{-3}$.

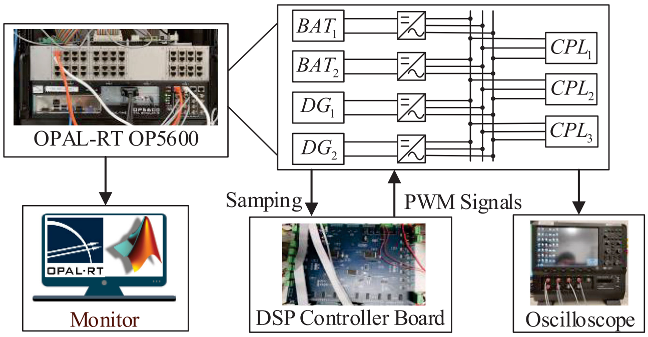

Fig. 23. CHIL experiment topology.

VI. Experimental Results

In order to verify the performance of the proposed adaptive step search strategy, the controller hardware-in-the-loop (CHIL) experiments are executed in the OPAL-RT real-time simulation system with the system parameters shown in Table I. The CHIL experiment facility is cited in our previous literature [33]. The detailed sections are shown as follows: To validate the proposed stability region approach for stand-alone supply systems with CPLs, an in-house controller HIL experimental platform is built as in Fig. 23, and its control frequency is 10^5 Hz. Each battery model is controlled through Digital Signal Processor (DSP) controllers (TMS320F28335). Therein, the inputs of DSPs are three-phase voltage and current measurements, which are converted from digital signals to the analog signals by the D2A terminals of OPAL-RT system. Meanwhile, the outputs of the DSP controllers are pulsewidth modulation (PWM) signals, which are sent to the PWM channels of the OPAL-RT system and then drive the power switches in the battery inverter models. Finally, the switching models of the other components and their associated controllers are embedded into OPAL-RT OP5600 simulator to represent the load subsystem. Therein, the rated capacities of the first CPL, the second CPL, and the third CPL are 18, 9, and 9 kW, respectively. And the rated capacity of each DG is 10 kW.

The droop coefficients of these two batteries and other parameters are the same as that in Section V-B. Assume that the active/reactive droop coefficients of the second battery are also unchanged. As a result, the droop coefficients stability region is also shown in Fig. 15 where the stability region is green area. First and foremost, the droop coefficients of the first battery are $m_{P1} = 2 \times 10^{-4}$ and $n_{Q1} = 3.4 \times 10^{-3}$. Under this case, the droop coefficients point is located in the green area of Fig. 15, which illustrates that the stand-alone supply system will be stable. As shown in Fig. 24, the three-phase experimental voltage is stable. Therein, the experimental result is in accordance with the conclusion of the proposed adaptive step search strategy. Furthermore, the droop coefficients of the first battery are changed from $m_{P1} = 2 \times 10^{-4}$ and $n_{Q1} = 3.4 \times 10^{-3}$ to $m_{P1} = 2 \times 10^{-3}$ and $n_{Q1} = 3.4 \times 10^{-2}$, which is caused through the foresaid reason in the Section V-B. Under this case, the droop coefficients point is outside stability region. Thus, it is possible that the stand-alone supply system is unstable. As shown in Fig. 25, the stand-alone supply system is unstable. Moreover, the reactive droop coefficient is also chosen as $n_{Q1} = 3.4 \times 10^{-3}$. Meanwhile, the active droop coefficient m_{P1} is variable, and its change is based on Fig. 26. Before T_1, droop coefficients point is located into stability region, which is shown in Fig. 15, and the stand-alone supply system must be stable. Furthermore, after T_1, droop coefficients point is outside stability region. Under this case, it is possible that the stand-alone supply system is unstable. As shown in Fig. 27, three-phase voltage experiment waveform is in accordance with the proposed stability region identification strategy. To sum up, the effectiveness of the proposed adaptive step search strategy based on generalized incidence matrix is verified through experimental results.

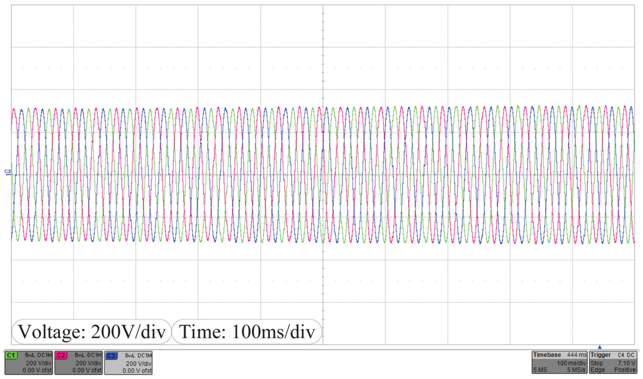

Fig. 24. Three-phase voltage experimental waveform under $m_{P1} = 2 \times 10^{-4}$ and $n_{Q1} = 3.4 \times 10^{-3}$.

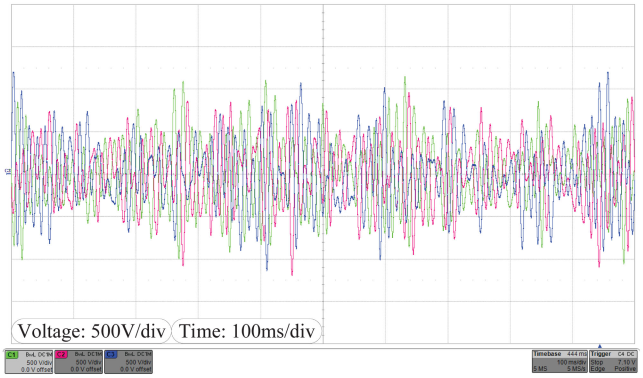

Fig. 25. Three-phase voltage experimental waveform under $m_{P1} = 2 \times 10^{-3}$ and $n_{Q1} = 3.4 \times 10^{-2}$.

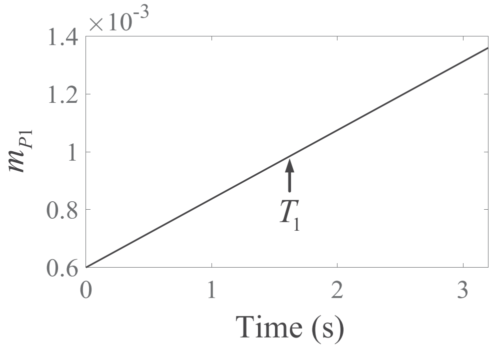

Fig. 26. Variation curve regarding droop coefficient in experiment.

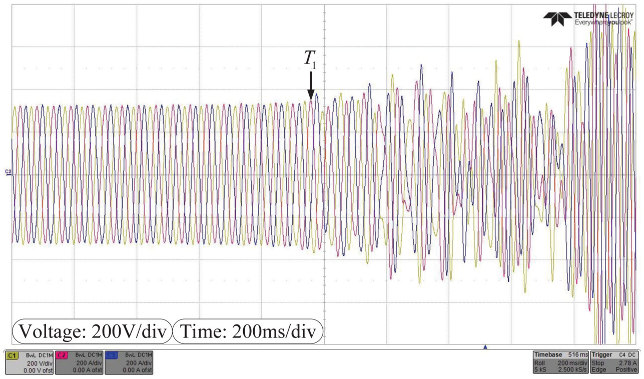

Fig. 27. Three-phase voltage experiment waveform under variable droop coefficients.

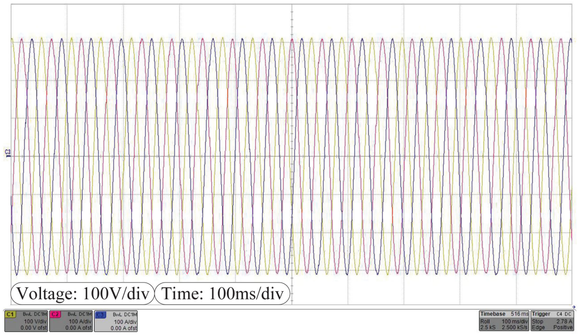

Fig. 28. Three-phase voltage experimental waveform under $m_{P1} = 8 \times 10^{-4}$ and $n_{Q1} = 3.4 \times 10^{-3}$.

Furthermore, The total rating of DG is changed from 20 to 30 kW. Under this case, the droop coefficients stability region based on the proposed adaptive step search strategy is also shown in Fig. 20 where the stability region is green area. First, the droop coefficients of the first battery are $m_{P1} = 8 \times 10^{-4}$ and $n_{Q1} = 3.4 \times 10^{-3}$. Based on this, the droop coefficients point is located in green area of Fig. 20, which illustrates that the stand-alone supply system must be stable. As shown in Fig. 28, the three-phase voltage is stable. Furthermore, the droop coefficients of the first battery are changed as $m_{P1} = 1.2 \times 10^{-3}$ and $n_{Q1} = 3.4 \times 10^{-3}$. Under this case, the droop coefficients point is outside stability region. As a result, it is possible that the stand-alone supply system is unstable. As shown in Fig. 29, the instability phenomenon has occurred in the stand-alone supply system. Thus, the performance of the proposed approach can be verified through the foresaid experiment results.

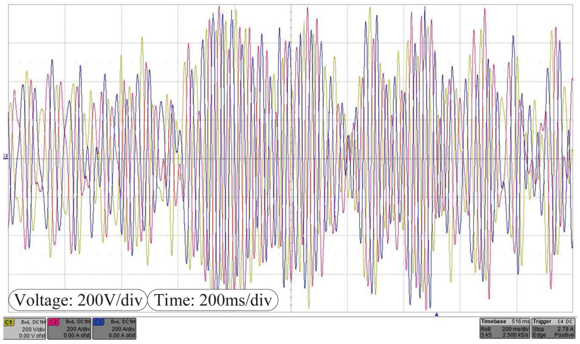

Fig. 29. Three-phase voltage experimental waveform under $m_{P1} = 1.2 \times 10^{-3}$ and $n_{Q1} = 3.4 \times 10^{-3}$.

VII. CONCLUSION

In order to eliminate the intercommunication modes, the droop controlled batteries have been widely applied in the stand-alone supply system, which results in small-signal instability problem. Although the impedance approach has been studied to assess the system stability, it cannot provide the stability region of droop coefficients varying with the battery SoC and charge/discharge mode. Consequently, this article has proposed a droop coefficients stability region analysis approach based on the generalized incidence matrix. Compared with the existing literatures, four advantages have been found in this article as follows.

1) The novel stability forbidden/operation region criterion has been proposed, resulting in lower conservatism than the partial stability forbidden region criteria and the norm-based impedance criteria. Meanwhile, the proposed criterion has similar conservatism with N-FRB criterion;
2) The interactive stability subregion has been first switched as Hurwitz matrix identification problem through the rotation mapping and translation mapping, which simplifies the calculation process.
3) Combining state matrix and equivalent return-ratio matrix, the generalized incidence matrix has been first constituted to simultaneously identify the subsystem stability and interactive stability.
4) Based on the generalized incidence matrix, this article has proposed an adaptive step search strategy to obtain the droop coefficients stability region, which provides the guidance for the energy management of batteries and stabilization method research works.

Finally, the simulation and CHIL experimental results have been provided to verify the conservatism and effectiveness.

REFERENCES

[1] A. Urtasun, A. Berrueta, P. Sanchis, and L. Marroyo, “Parameter-independent control for battery chargers based on virtual impedance emulation,” *IEEE Trans. Power Electron.*, vol. 33, no. 10, pp. 8848–8858, Oct. 2018.

[2] R. Wang, Q. Sun, D. Ma, and Z. Liu, "The small-signal stability analysis of the droop-controlled converter in electromagnetic timescale," *IEEE Trans. Sustain. Energy*, vol. 10, no. 3, pp. 1459–1469, Jul. 2019.

[3] L. Zhang, X. Ruan, and X. Ren, "Second-harmonic current reduction for two-stage single-phase inverter with boost-derived front-end converter: Control schemes and design considerations," *IEEE Trans. Power Electron.*, vol. 33, no. 7, pp. 63618–C6378, Jul. 2018.

[4] K. A. Potty, E. Bauer, H. Li, and J. Wang, "Smart resistor: Stabilization of DC microgrids containing constant power loads using high-bandwidth power converters and energy storage," *IEEE Trans. Power Electron.*, vol. 35, no. 1, pp. 957–967, Jan. 2020.

[5] A. Urtasun, P. Sanchis, and L. Marroyo, "State-of-charge-based droop control for stand-alone systems with distributed energy storage," *Energy Convers. Manage.*, vol. 106, pp. 709–720, Dec. 2015.

[6] X. Meng, J. Liu, and Z. Liu, "A generalized droop control for grid-supporting inverter based on comparison between traditional droop control and virtual synchronous generator control," *IEEE Trans. Power Electron.*, vol. 34, no. 6, pp. 5416–5438, Jun. 2019.

[7] E. K. Belal, D. M. Yehia, and A. M. Azmy, "Adaptive droop control for balancing SOC of distributed batteries in DC microgrids," *IET Gener., Transmiss. Distrib.*, vol. 13, no. 20, pp. 4667–4676, Oct. 2019.

[8] A. Kunwar, F. Shahnia, and R. C. Bansal, "Eigenvalue-oriented dynamic stability examination to enhance designing a microgrid hosting clusters of inertial and non-inertial distributed generators," *IEEE Trans. Smart Grid*, vol. 11, no. 3, pp. 1942–1955, May 2020.

[9] E. A. A. Coelho, P. C. Cortizo, and P. F. D. Garcia, "Small-signal stability for parallel-connected inverters in stand-alone AC supply systems," *IEEE Trans. Ind. Appl.*, vol. 38, no. 2, pp. 533–542, Mar./Apr. 2002.

[10] N. Pogaku, M. Prodanovic, and T. C. Green, "Modeling, Analysis and testing of autonomous operation of an inverter-based microgrid," *IEEE Trans. Power Electron.*, vol. 22, no. 2, pp. 613–625, Mar. 2007.

[11] Z. Li and M. Shahidehpour, "Small-signal modeling and stability analysis of hybrid AC/DC microgrids," *IEEE Trans. Smart Grid*, vol. 10, no. 2, pp. 2080–2095, Mar. 2019.

[12] Y. Wang, X. Wang, F. Blaabjer, and Z. Chen, "Harmonic instability assessment using state-space modeling and participation analysis in inverter-fed power systems," *IEEE Trans. Ind. Electron.*, vol. 64, no. 1, pp. 806–816, Jan. 2017.

[13] V. Purba, B. B. Johnson, M. Rodriguez, S. Jafarpour, F. Bullo, and S. V. Dhople, "Reduced-order aggregate model for parallel-connected single-phase inverters," *IEEE Trans. Energy Convers.*, vol. 34, no. 2, pp. 824–837, Jun. 2019.

[14] W. Cao, Y. Ma, L. Yang, F. Wang, and L. M. Tolbert, "D-q impedance based stability analysis and parameter design of three-phase inverter-based AC power systems," *IEEE Trans. Ind. Electron.*, vol. 64, no. 7, pp. 6017–6028, Jul. 2017.

[15] C. Zhang, M. Molinas, A. Rygg, J. Lyu, and X. Cai, "Harmonic transfer-function-based impedance modeling of a three-phase VSC for asymmetric AC grid stability analysis," *IEEE Trans. Power Electron.*, vol. 34, no. 12, pp. 12552–12566, Dec. 2019.

[16] W. Wu *et al.*, "Sequence impedance modeling and stability comparative analysis of voltage-controlled VSGs and current-controlled VSGs," *IEEE Trans. Ind. Electron.*, vol. 66, no. 8, pp. 6460–6472, Aug. 2019.

[17] F. Liu, J. Liu, H. Zhang, and D. Xue, "Stability issues of $Z + Z$ type cascade system in hybrid energy storage system (HESS)," *IEEE Trans. Power Electron.*, vol. 29, no. 11, pp. 5846–5859, Nov. 2014.

[18] A. Rygg and M. Molinas, "Apparent impedance analysis: A. small-signal method for stability analysis of power electronic-based systems," *IEEE J. Emerg. Sel. Topics Power Electron.*, vol. 5, no. 4, pp. 1474–1486, Dec. 2017.

[19] X. Wang and F. Blaabjerg, "Harmonic stability in power electronic-based power systems: Concept, modeling, and analysis," *IEEE Trans. Smart Grid*, vol. 10, no. 3, pp. 2858–2870, May 2019.

[20] Z. Liu, J. Liu, W. Bao, and Y. Zhao, "Infinity-norm of impedance-based stability criterion for three-phase AC distributed power systems with constant power loads," *IEEE Trans. Power Electron.*, vol. 30, no. 6, pp. 3030–3043, Jun. 2015.

[21] A. Riccobono and E. Santi, "Comprehensive review of stability criteria for DC power distribution systems," *IEEE Trans. Ind. Appl.*, vol. 50, no. 5, pp. 3525–3535, Sep./Oct. 2014.

[22] X. Li, X. Ruan, Q. Jin, M. Sha, and C. K. Tse, "Small-signal models with extended frequency range for DC-DC converters with large modulation ripple amplitude," *IEEE Trans. Power Electron.*, vol. 33, no. 9, pp. 8151–8163, Sep. 2018.

[23] Y. Zhou, H. Hu, J. Yang, and Z. He, "A novel forbidden-region-based stability criterion in modified sequence-domain for AC grid-converter system," *IEEE Trans. Power Electron.*, vol. 34, no. 4, pp. 2988–2995, Apr. 2019.

[24] X. Zhang, X. Ruan, and C. K. Tse, "Impedance-based local stability criterion for DC distributed power systems," *IEEE Trans. Circuits Syst. I., Reg. Papers*, vol. 62, no. 3, pp. 916–925, Mar. 2015.

[25] J. Chen and J. Chen, "Stability analysis and parameters optimization of islanded microgrid with both ideal and dynamic constant power loads," *IEEE Trans. Ind. Electron.*, vol. 65, no. 4, pp. 3263–3274, Apr. 2018.

[26] A. A. A. Radwan and Y. A. R. I. Mohamed, "Analysis and active-impedance-based stabilization of voltage-source-rectifier loads in grid-connected and isolated microgrid applications," *IEEE Trans. Sustain. Energy*, vol. 4, no. 3, pp. 563–576, Jul. 2013.

[27] L. Huang *et al.*, "Grid-synchronization stability analysis and loop shaping for PLL-based power converters with different reactive power control," *IEEE Trans. Smart Grid*, vol. 11, no. 1, pp. 501–516, Jan. 2020, doi: 10.1109/TSG.2019.2924295.

[28] Z. Shuai, Y. Li, W. Wu, C. Tu, A. Luo, and Z. J. Shen, "Divided DQ small-signal model: A new perspective for the stability analysis of three-phase grid-tied inverters," *IEEE Trans. Ind. Electron.*, vol. 66, no. 8, pp. 6493–6504, Aug. 2019.

[29] Shuoh Rern, P. T.Kabamba, and D. S.Bernstein, "Guardian map approach to robust stability of linear systems with constant real parameter uncertainty," *IEEE Trans. Autom. Control*, vol. 39, no. 1, pp. 162–164, Jan. 1994.

[30] X. Guo, Z. Lu, B. Wang, X. Sun, L. Wang, and J. M. Guerrero, "Dynamic phasors-based modeling and stability analysis of droop-controlled inverters for microgrid applications," *IEEE Trans. Smart Grid*, vol. 5, no. 6, pp. 2980–2987, Nov. 2014.

[31] A. Li and D. Zhang, "Necessary and sufficient stability criterion and new forbidden region for load impedance specification," *Chin. J. Electron.*, vol. 23, no. 3, pp. 628–634, Jul. 2014.

[32] J. Liu, X. Feng, F. C. Lee, and D. Borojevich, "Stability margin monitoring for DC distributed power systems via perturbation approaches," *IEEE Trans. Power Electron.*, vol. 18, no. 6, pp. 1254–1261, Nov. 2003.

[33] P. Lin *et al.*, "A distributed power management strategy for multi-paralleled bidirectional interlinking converters in hybrid AC/DC microgrids," *IEEE Trans. Smart Grid*, vol. 10, no. 5, pp. 5696–5711, Sep. 2019.

Rui Wang (Student Member, IEEE) received the B.S. degree in electrical engineering and automation in 2016 from Northeastern University, Shenyang, China, where he is currently working toward the Ph.D. degree in power electronics and power drive.

Since 2019, he has become a Visiting Scholar with the Energy Research Institute, Nanyang Technological University, Singapore. He has authored or coauthored more than 40 papers, and has authorized more than ten invention patents. His research interests focus on modeling of distributed renewable energy source in microgrid, stability analysis approach and stabilizing control strategy for microgrid, smart grid, and so on.

Qiuye Sun (Senior Member, IEEE) received the Ph.D. degree in control science and engineering from Northeatern University, Liaoning, China, in 2007.

He is currently a Full Professor with Northeastern University. He has authored or coauthored more than 200 papers, authorized more than 100 invention patents, and authored or coauthored more than ten books or textbooks. His current research interests include optimization analysis technology of power distribution network, network control of energy Internet, integrated energy systems and microgrids.

Dr. Sun is an IET fellow and an Associate Editor for the IEEE TRANSACTIONS ON NEURAL NETWORKS AND LEARNING SYSTEMS, *IET Cyber-Physical Systems*, *CSEE Journal of Power and Energy Systems*, IEEE/CAA JOURNAL OF AUTOMATICA SINICA, *International Transactions on Electrical Energy Systems*, and so on.

Wei Hu (Student Member, IEEE) received the B.Eng. and M.Sc. degrees in electrical engineering from Harbin Institute of Technology, Harbin, China, in 2014 and 2016, respectively, and the Ph.D. degree in electrical engineering from Zhejiang University, Hangzhou, China, in 2020.

He is currently an Assistant Professor with the College of Mechanical and Vehicle Engineering, Hunan University, Hunan, China. His current main research interests focus on the structure and drives of open-winding permanent-magnet synchronous motor.

Yushuai Li (Member, IEEE) received the B.S. degree in electrical engineering and automation and the Ph.D. degree in control theory and control engineering from the Northeastern University, Shenyang, China, in 2014 and 2019, respectively.

From 2019 to 2020, he was a Postdoctoral Research Scholar with the Department of Electrical and Computer Engineering, University of Denver, Denver, CO, USA. He is currently a Lecturer with the School of Information Science and Engineering, Northeastern University. His main research interests include distributed modelling, control, energy management and optimization of energy Internet and multienergy systems, as well as distributed machine learning algorithm with applications in microgrids.

Dr. Li is currently an Editor for *Frontiers in Energy Research*. He is the Section Chair for the IEEE 4th Conference on Energy Internet and Energy System Integration.

Dazhong Ma (Member, IEEE) received the B.S. degree in automation and the Ph.D. degree in control theory and control engineering from Northeastern University, Shenyang, China, in 2004 and 2011, respectively.

He is currently an Associate Professor with the Northeastern University. His current research interests include fault diagnosis, fault-tolerant control, energy management systems, control and optimization of distributed generation systems, microgrids, and energy Internet.

Peng Wang (Fellow, IEEE) received the B.Sc. degree in electronic engineering from Xian Jiaotong University, Xian, China, in 1978, the M.Sc. degree from Taiyuan University of Technology, Taiyuan, China, in 1987, and the M.Sc. and Ph.D. degrees in electrical engineering from the University of Saskatchewan, Saskatoon, SK, Canada, in 1995 and 1998, respectively.

He is currently a Full Professor with the School of Electrical and Electronic Engineering, Nanyang Technological University, Singapore. His current research interests include power system planning and operation, renewable energy planning, solar/electricity conversion system, and power system reliability analysis.

Dr. Wang is currently an Associate Editor or Guest Editor-in-Chief for the IEEE TRANSACTIONS ON SMART GRID, IEEE TRANSACTIONS ON POWER DELIVERY, *Journal of Modern Power Systems and Clean Energy*, *CSEE Journal of Power and Energy Systems*, and so on.